DOI: 10.13009/EUCASS2017-157

Development of an Eddy Dissipation Model for the use in Numerical Hybrid Rocket Engine Combustion Simulation

Stefan May, Sebastian Karl** and Ognjan Božić**

** DLR - German Aerospace Center, Institute of Aerodynamics and Flow Technology, Department Spacecraft*

Lilienthalplatz 7, 38108 Braunschweig, Germany, stefan.may@dlr.de, ognjan.bozic@dlr.de

*** DLR - German Aerospace Center, Institute of Aerodynamics and Flow Technology, Department Spacecraft*

Bunsenstraße 10, 37073 Göttingen, Germany, sebastian.karl@dlr.de

Abstract

Within this work, an Eddy Dissipation Model for the combustion process in hybrid rocket engines was developed and implemented into the DLR TAU-Code. The model was developed especially for the propellant combination of hydroxyl-terminated polybutadiene and high concentrated hydrogen peroxide. A numerical generic hybrid rocket combustion chamber was designed to compare the results of the Eddy Dissipation Model simulations with Arrhenius based combustion models. For example, the well validated multistage combustion model from Westbrook and Dryer was applied. The results of the Eddy Dissipation Model simulations are very close to the multistage combustion results and require significantly reduced computing time.

1. Introduction

In the last few years, the development and research on hybrid rocket engines (HRE) is subject of increased research effort. This is due to the possible combination of the advantages of solid rocket motors as well as liquid rocket engines (LRE). HRE are thrust controllable and re-ignitable. Since only one fluid must be stored and conducted into the combustion chamber, the constructive buildup is relatively simple and therefore cheaper than for LRE. In addition, common propellant combinations are environmentally safe without production of acids and some oxidizers, like high concentrated hydrogen peroxide (so called “high test peroxide” - HTP), are non-cryonic. The main disadvantages of HRE are the strong dependency of the regression rate on local conditions like local oxidizer presence and local heat transfer from the hot gas to the fuel surface and in addition, the shifts of free streaming cross section and fuel surface during the combustion process. Through this behavior, most in the past realized HRE have low averaged combustion efficiency over the whole combustion time.

Within the AHRES (Advanced Hybrid Rocket Engine Simulation) program of the German Aerospace Center (DLR), the Institute of Aerodynamics and Flow Technology is developing a software environment for the design of hybrid rocket engines [1]. For the validation of this software, the Department Spacecraft is operating a lab-scale hybrid rocket engine for ground tests at the DLR test area in Trauen, Germany. The engine is propelled with HTP (87.5 wt.%) as liquid oxidizer and hydroxyl-terminated polybutadiene (HTPB), pure or with different metallic additives, as solid fuel. Since the time accurate flow conditions within HRE are not measureable, numerical simulations of the flow and combustion inside of HRE are necessary to determine the local conditions on the fuel surface and in consequence to increase the regression rate and the combustion efficiency.

The numerical simulations are performed with the chemical non-equilibrium version of the DLR TAU-Code. Based on Arrhenius equations, it is possible to implement very complex chemical reaction mechanisms. Up to now, several steady-state simulations, realized with the multistep combustion model of Westbrook and Dryer [2] are carried out and the results show very good agreement with firing tests [3, 4]. But with respect to the needed computing capacity and time, it is very expensive to realize 3D calculations – not to mention the realization of unsteady combustion simulations. Therefore, an Eddy Dissipation Model (EDM) was implemented to reduce the needed computational capacity but with the aim to achieve a sufficient exact flow and combustion process.

DOI: 10.13009/EUCASS2017-157

2. Simulation settings

The DLR TAU-Code is a powerful numerical simulation platform for several kinds of flow fields. Calculations with the Euler or the Navier-Stokes solver, with upwind or central discretization and with different numerical solver methods are feasible. In addition, different one- and two-equation turbulence models as well as LES and DES methods are available and the chemistry module contains appropriate models for re-entry, real gas and combustion calculations.

The version of the DLR TAU-Code which was used for the present work implements reaction models for chemical non-equilibrium conditions. Since the Arrhenius equations are highly non-linear and stiff, which implies a numerical unstable behavior, it is necessary to use a stable method to solve the Navier-Stokes equations. Therefore, a point implicit method for the chemical source terms in conjunction with a Runge Kutta method for the integration of the governing equations was used. The flow field is spatial discretized by a second order upwind scheme and for the turbulence modeling, the Menter-SST model [5] was used.

2.1 Computational mesh

For the comparison of the combustion models, a generic hybrid rocket engine was designed. This engine is mapped with a 2.5 dimensional rotation-symmetrical mesh. Due to the relative simple geometry, it is possible to realize a couple of different calculations with an, for this purpose, acceptable amount of combustion capacity and time. The used computational hybrid mesh is generated with the meshing program CENTAUR. Hybrid mesh means, that the boundary layer is discretized with structured cells (rectangles), while the remaining part of the flow field is meshed with unstructured cells (triangles). The number of nodes for the used computational mesh is around 35 000. In Fig. 1, the used mesh is shown. It is obvious that the resolution of the mesh is very dense in comparison to the size of the flow field. That is justified, because the chemical reaction model is very temperature sensitive (see Chapter 3) and therefore, high temperature gradients would break off the calculation process. The boundary layer is resolved with 40 points normal to the wall and the averaged y^+ is around 0.5.

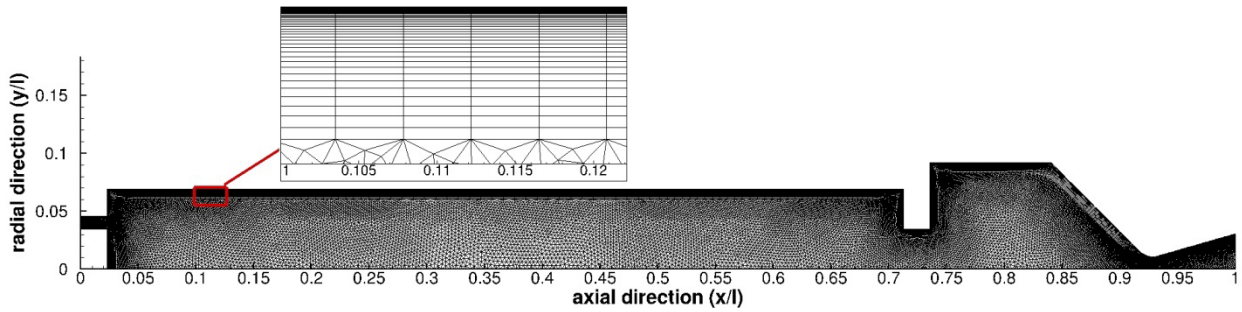

Figure 1: 2.5D hybrid mesh for the comparison of different combustion models

2.2 Boundary conditions

For the definition of the flow field, different boundary conditions are applied, shown in Fig. 2. Within the simulation, hot oxygen and overheated water vapor are introduced into the combustion chamber through the injector plate. That is justified, because during the real engine operation, the HTP will be decomposed completely through the catalyst chamber before it is injected into the combustion chamber. For more information about the catalyst chamber, see [6, 7]. The composition and conditions of the mass flux are used with respect to the adiabatic decomposition of 87.5 %wt. HTP. The injector plate is modeled by a reservoir inflow boundary condition, where the total pressure, the density at total conditions as well as the mass flux is defined. The used values are summarized in Table 1.

The modeling of the fuel pyrolysis process along the reaction surface is simplified. For lack of a superior boundary condition, the fuel surface is assumed as viscous porous wall and purely gaseous 1,3-Butadiene (C_4H_6) is injected through this wall. According to Chiaverini et al. [8], 1,3-Butadiene is the main pyrolysis product of HTPB. Therefore, it was used as the only fuel component to reduce the overall computing time of the simulation. With respect to [9], a typical pyrolysis temperature for lab scale HRE is around 1050 K. Since a local surface condition is not adjustable with the used boundary condition, the wall temperature is assumed to be constant and set to this pyrolysis temperature. In addition, the mass flux is assumed to be constant along the complete surface of the solid

DOI: 10.13009/EUCASS2017-157

grain. The used mass flows and pressure conditions are taken from experiments carried out by Porrmann et al. [10]. The boundary parameters are summarized in Table 2.

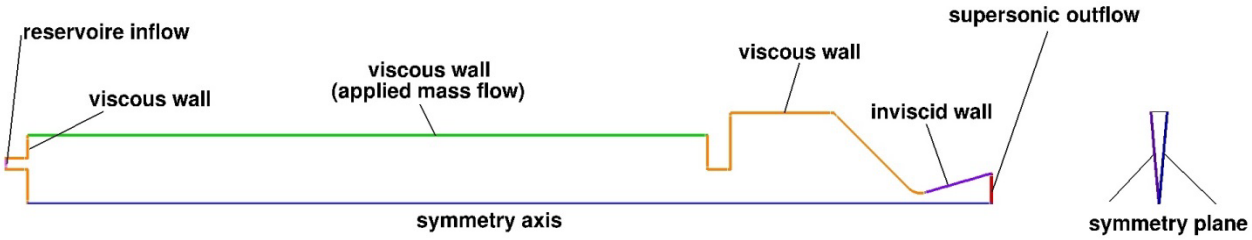

Figure 2: Used boundary conditions for the generic HRE

Table 1: Used parameters and values for the oxidizer inflow boundary condition

Parameter	Value	Unit
Total pressure	5 000 000	N/m^2
Total density	13.64	kg/m^3
Oxidizer mass flux	327.6	$kg/(s \cdot m^2)$
Mass fraction H_2O	0.588	-
Mass fraction O_2	0.412	-

Table 2: Used parameters and values for the fuel boundary condition

Parameter	Value	Unit
Fuel mass flux	0.455	$kg/(s \cdot m^2)$
Mass fraction C_4H_6	1.0	-
Isothermal wall temperature	1050	K

The outflow of the flow field is set at the nozzle outlet. Therefore, the entire nozzle expansion is considered. To achieve a “clean” simulation boundary, a supersonic outflow boundary condition was used and the divergent nozzle part is assumed as an adiabatic, non-viscous wall. The remaining solid walls (the inflow area upstream of the fuel, the post-combustion chamber as well as the convergent nozzle part and nozzle throat) are modeled as adiabatic, viscous walls. Radiation influence between the gas flow and the walls as well as between different gas layers is not considered.

3. Chemical reaction models

As described in the introduction, the in TAU implemented Arrhenius based reaction mechanism can describe the combustion process very exact by the possible implementation of hundreds of chemical reaction equations, which are including a lot of different species. But for each species, an own continuity equation has to be solved within the coupled system of the Navier-Stokes equations and therefore this kind of calculation requires a very high computational capacity. To reduce the needed computational capacity and time, an EDM for the combustion process in HRE based on HTPB and HTP was developed and implemented into the TAU code.

DOI: 10.13009/EUCASS2017-157

3.1 Arrhenius based combustion model

For the comparison with the EDM, the reaction mechanism derived from the work of Westbrook and Dryer (WD) [2] is used. It is a multistage combustion model with a quasi-global first reaction step for the reaction of 1,3-Butadiene with oxygen. This reaction mechanism delivers good results by an acceptable calculation effort. The combustion process chain is modeled by 22 kinetic reactions under consideration of 12 different reaction species. All reaction equations and the related parameters are summarized in Table 3. These parameters are displayed completely in SI units. Within the TAU code, they are applied within modified Arrhenius equations of the following form:

$$k_R = A \cdot T^B \cdot exp\left(-\frac{C}{T}\right) \tag{1}$$

With this equation, the reaction rates k_R and therefore the source and sink terms for all species are determined for each calculation step. The backward reaction rate is computed from the equilibrium constant and the chemical source terms are determined by the law of mass action. To expect from Eq. (1), the reaction rates strongly depend on the local temperature *T*. The temperature of the fluid is calculated from the local total energy of the flow through the change of sensible enthalpy of each reaction. This is determined through the differences of the enthalpy of formation of each produced or consumed species. The properties of each species (e.g. heat of formation, molar mass, viscosity and heat capacity) are generated with the database of the NASA CEA code [11].

3.2 Eddy Dissipation Model

The in TAU implemented combustion model based on the Eddy Break-Up Model developed by Spalding [12], which was improved to the EDM by Magnussen [13]. The model postulates that the reaction only occurs if the breakup of the turbulent structures reaches the finest turbulent scales. Combined with the underlying assumption that the chemical reaction rate is significant faster compared to the breakup of turbulent structures (fast chemistry assumption), it implies that the reaction will carried out just in time when the finest turbulent scales are reached. Therefore, the reaction rate can be described by common parameters of two-equation-models: the turbulent dissipation rate ε and the turbulent kinetic energy *k*. The quotient of these two values represents a characteristic turbulent time scale. By using of *k*-ω turbulence models, it will calculate to

$$\frac{\varepsilon}{k} = c_\mu \cdot \omega \cdot F \tag{2}$$

with a factor c_μ=0.09. To achieve the correct combustion rate, the empirical factor *F* was introduced. For the current calculations, it was set to 10. The fast chemistry assumption presupposes high temperatures or pressures. If these conditions are not fulfilled, the realistic chemical reaction rates are relative slow and in that case, the EDM produces significant errors. In the presented application case for the combustion in HRE with a HTP/HTPB propellant combination, the HTP will completely decompose into free oxygen and water steam with temperatures about 900 K before it will be entering the combustion chamber. Therefore, for the combustion simulation this hot gas composition is introduced into the simulation area and so, high temperatures are ensured and the fast chemistry assumption is fulfilled on each location. The implemented reaction equation for the described HRE combustion is:

$$C_4H_6 + n_y \cdot O_2 \rightarrow n_z \cdot Prod \tag{3}$$

Prod is a model specie for the combustion products. This specie as well as the factors n_y and n_z depending on the global oxidizer to fuel (O/F) ratio and have to be trimmed to the expected relation to achieve a high combustion quality. The composition of *Prod* and the values for n_y and n_z are calculable with the NASA CEA code [11]. For the here chosen O/F ratio of 7.0, Eq. (3) is formulated as:

DOI: 10.13009/EUCASS2017-157

$$C_4H_6 + 4.87 \cdot O_2 \rightarrow 7.3 \cdot Prod \quad \textbf{(4)}$$

The composition of *Prod* is summarized in Table 4. Corresponding to this composition, the thermal and transport properties of this specie is calculated with mixing rules for ideal gases.

Table 3: Chemical reaction model for the non-equilibrium calculations (units in meter, mol, second and kilogram) [2]

No.	Reaction	A	B	$C = {E_a}/{R_u}$
1	$C_4H_6 + 2O_2 \rightarrow 4CO + 3H_2$	$4.1 \cdot 10^7$	0	$15.107 \cdot 10^3$
2	$H + O_2 \rightarrow O + OH$	$2.2 \cdot 10^8$	0	$8.460 \cdot 10^3$
3	$H_2 + O \rightarrow H + OH$	$1.8 \cdot 10^4$	1.0	$4.482 \cdot 10^3$
4	$O + H_2O \rightarrow OH + OH$	$6.8 \cdot 10^7$	0	$9.265 \cdot 10^3$
5	$OH + H_2 \rightarrow H + H_2O$	$2.2 \cdot 10^7$	0	$2.568 \cdot 10^3$
6	$H + O_2 + M \rightarrow HO_2 + M$	$1.5 \cdot 10^3$	0	$-0.504 \cdot 10^3$
7	$O + HO_2 \rightarrow O_2 + OH$	$5.0 \cdot 10^7$	0	$0.504 \cdot 10^3$
8	$H + HO_2 \rightarrow OH + OH$	$2.5 \cdot 10^8$	0	$0.957 \cdot 10^3$
9	$H + HO_2 \rightarrow O_2 + H_2$	$2.5 \cdot 10^7$	0	$0.352 \cdot 10^3$
10	$OH + HO_2 \rightarrow H_2O + O_2$	$5.0 \cdot 10^7$	0	$0.504 \cdot 10^3$
11	$HO_2 + HO_2 \rightarrow H_2O_2 + O_2$	$1.0 \cdot 10^7$	0	$0.504 \cdot 10^3$
12	$H_2O_2 + M \rightarrow OH + OH + M$	$1.2 \cdot 10^{11}$	0	$22.912 \cdot 10^3$
13	$HO_2 + H_2 \rightarrow H_2O_2 + H$	$7.3 \cdot 10^5$	0	$9.417 \cdot 10^3$
14	$H_2O_2 + OH \rightarrow H_2O + HO_2$	$1.0 \cdot 10^7$	0	$0.906 \cdot 10^3$
15	$CO + OH \rightarrow CO_2 + H$	$1.5 \cdot 10^1$	1.3	$-0.403 \cdot 10^3$
16	$CO + O_2 \rightarrow CO_2 + O$	$3.1 \cdot 10^5$	0	$18.934 \cdot 10^3$
17	$CO + O + M \rightarrow CO_2 + M$	$5.9 \cdot 10^3$	0	$2.065 \cdot 10^3$
18	$CO + HO_2 \rightarrow CO_2 + OH$	$1.5 \cdot 10^8$	0	$11.934 \cdot 10^3$
19	$OH + M \rightarrow O + H + M$	$8.0 \cdot 10^{13}$	-1.0	$52.219 \cdot 10^3$
20	$O_2 + M \rightarrow O + O + M$	$5.1 \cdot 10^9$	0	$57.909 \cdot 10^3$
21	$H_2 + M \rightarrow H + H + M$	$2.2 \cdot 10^8$	0	$48.341 \cdot 10^3$
22	$H_2O + M \rightarrow H + OH + M$	$2.2 \cdot 10^{10}$	0	$52.873 \cdot 10^3$

M represents the species for each third-body-collision reaction

DOI: 10.13009/EUCASS2017-157

Table 4: Composition of the model specie *Prod* for an O/F ratio of 7.0

Component	Substance amount fraction
CO_2	0.416
H_2O	0.297
CO	0.132
H_2	0.090
O_2	0.015
OH	0.042
H	0.006
O	0.002

Additional requirements for the execution of a chemical reaction within a simulation step are:

- A sufficient amount of fuel is available.
- A sufficient amount of oxidizer is available.
- A sufficient amount of energy is available for the current reaction step.

The energy condition can be fulfilled with the assumption, that enough of the hot reaction products have to be available at the reaction scale. In summary, three consumption rates q, representing the different above mentioned conditions, are calculated, based on the partial densities ρ_i of the species. The total consumption rate for the fuel is the minimum of these three rates. In Eq. (5-8) the complete reaction mechanism is declared:

$$q_1 = K_1 \cdot \rho_{C4H6} \cdot \frac{\varepsilon}{k} \tag{5}$$

$$q_2 = K_1 \cdot \frac{\rho_{O2}}{n_x} \cdot \frac{\varepsilon}{k} \tag{6}$$

$$q_3 = K_2 \cdot \frac{\rho_{Prod}}{n_x + 1} \cdot \frac{\varepsilon}{k} \tag{7}$$

$$\frac{dm_{C4H6}}{dt} = -\min(q_1; q_2; q_3) \tag{8}$$

The semi-empirical constants K_1 and K_2 are obtained from [13]. They are estimated with the mass ratio of oxidizer and fuel and can be used to trim the reaction. The mass weighted factor n_x depends on the molar masses M of fuel and oxidizer:

$$n_x = n_y \cdot \frac{M_{O2}}{M_{C4H6}} \tag{9}$$

DOI: 10.13009/EUCASS2017-157

In addition to the three species C_4H_6, O_2 and *Prod*, H_2O is implemented as fourth inert specie. Through the decomposition of HTP in mostly H_2O, it has a very important part of the gas mixture and therefore, the influence on gas mixture properties is very important. Due to this, the EDM contains four species. Compared to the 12 species of the WD mechanism, a significant computing time reduction of around one order of magnitude is reached through the explicit reduction of species number and therefore the number of transport equations.

4. Simulation results

In Fig. 3, the temperature distribution and velocity streamline evolution in the generic HRE are shown, calculated with the WD mechanism (top) and the EDM (bottom). The simulation results are very close together; temperature maximums (flame zones) and eddies appear at the same locations. Differences are only visible at the streamline evolution behind the oxidizer injection as well as at the temperature maximum.

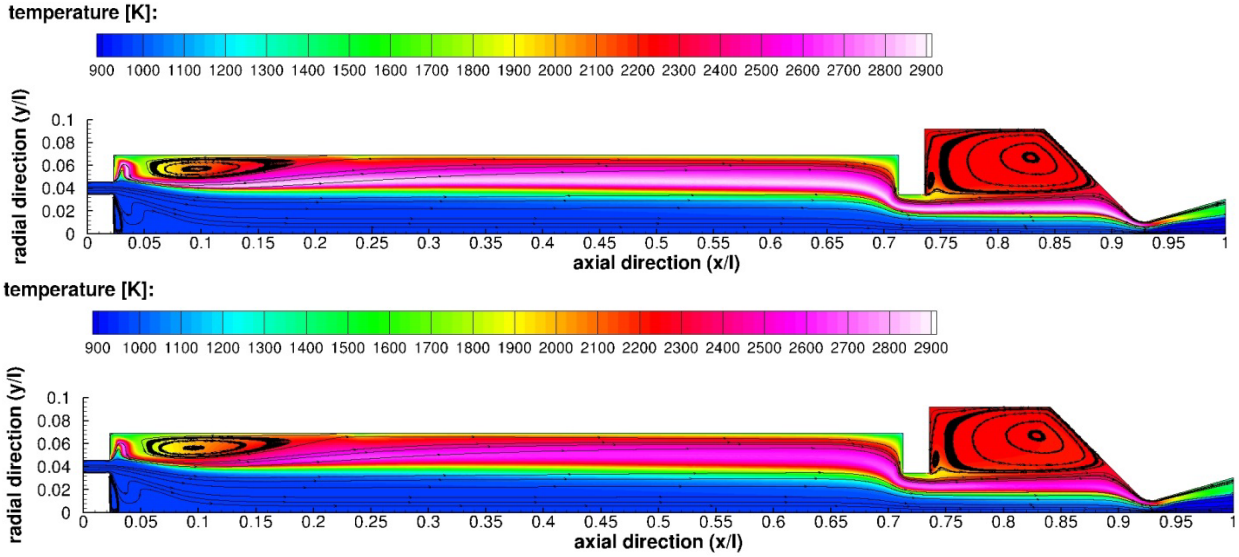

Figure 3: Temperature distribution and velocity streamline evolution within the generic HRE; top: Arrhenius based calculations withthe WD mechanism; bottom: calculations with the EDM

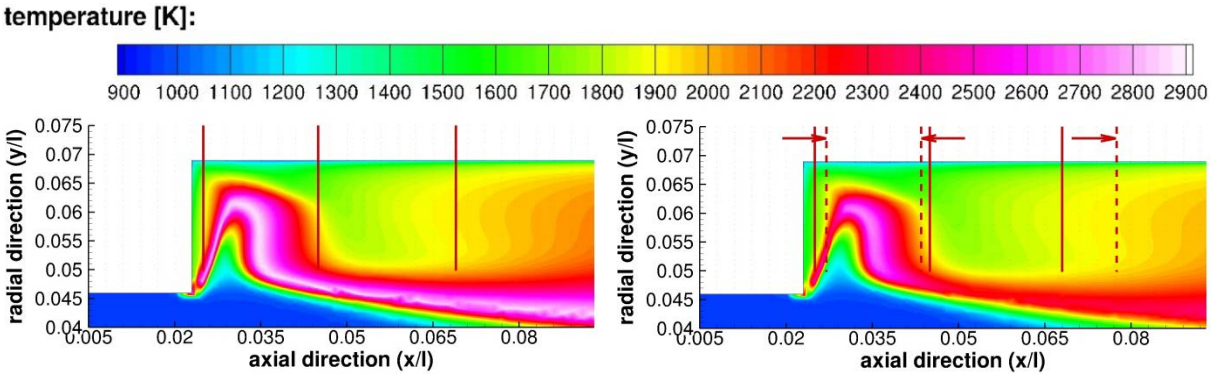

Figure 4: Temperature distribution detail near to the oxidizer injection; left: WD calculations; right: EDM calculations

Fig. 4 shows a detail of the oxidizer injection area. At the EDM calculation, the regions of temperature increasing (flame zones) are shifted slightly upstream and therefore the eddy development will be influenced. In addition, the hot regions are a bit smaller. Since the local shift is very small, also the influence at the occurring eddies is small. The effect of flame zone shift is significant reduced upstream of the flow field. Like shown in Fig. 5, differences in the flow field locations of the post combustion chamber are not visible and the temperature difference at all locations except the flame zone is smaller than 10 K.

DOI: 10.13009/EUCASS2017-157

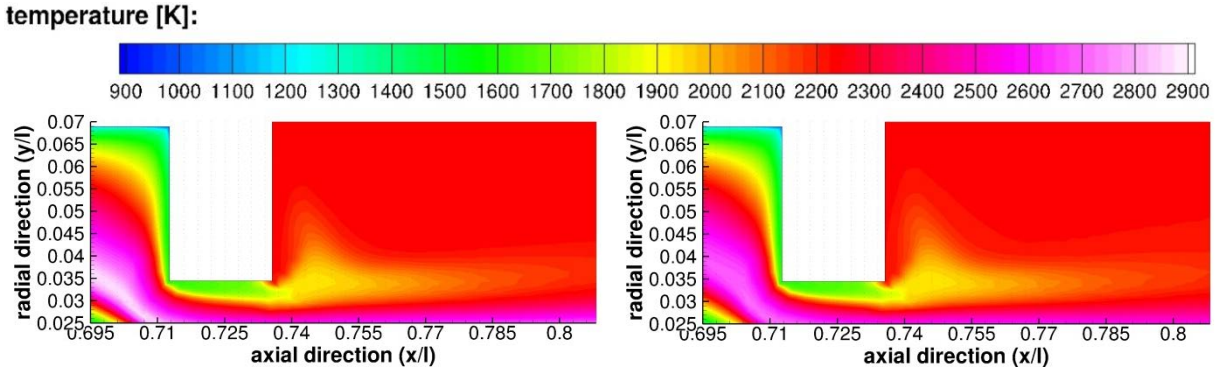

Figure 5: Temperature distribution detail at the post-combustion chamber entrance; left: WD mechanism; right: EDM

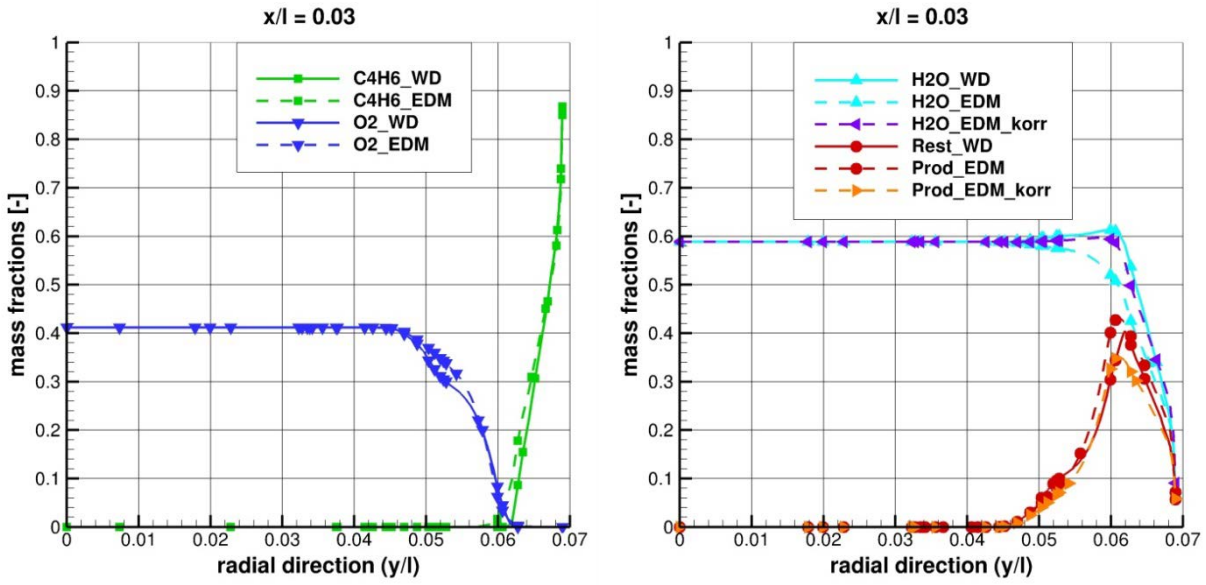

Figure 6: Comparison of the main reaction species distribution between the EDM and the WD mechanism in a axial cut at x/l=0.03 (injection area); left: C_4H_6 and O_2; right: H_2O and products

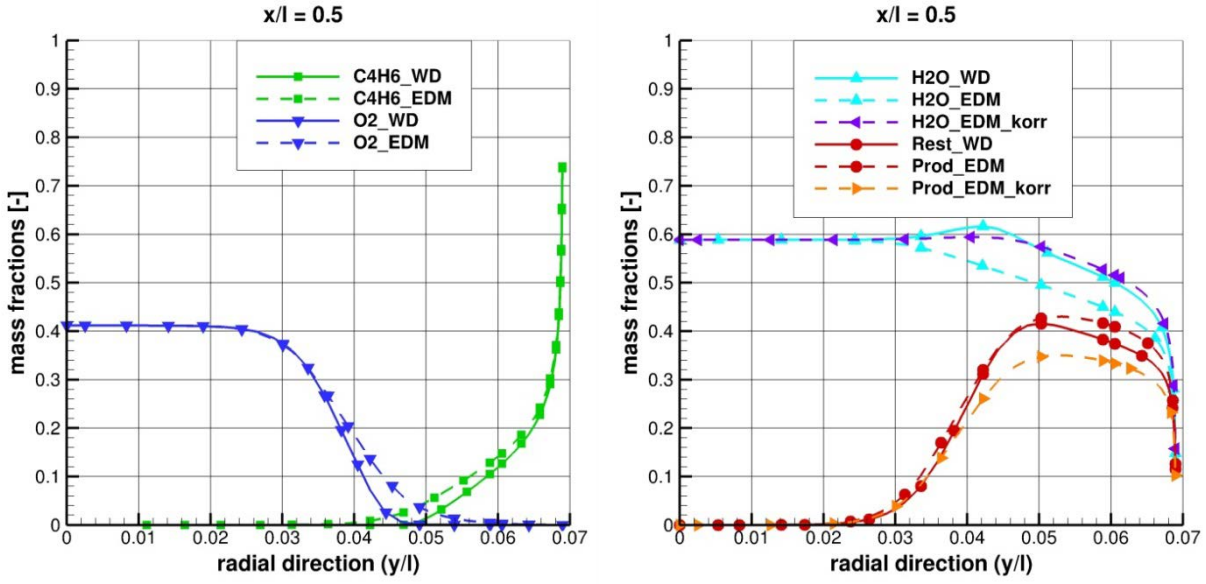

Figure 7: Comparison of the main reaction species distribution between the EDM and the WD mechanism in a axial cut at x/l=0.5 (combustion chamber); left: C_4H_6 and O_2; right: H_2O and products

DOI: 10.13009/EUCASS2017-157

The calculations with the EDM underestimate the maximum combustion temperature of around 100 K compared to the WD mechanism calculations. That is founded, because the combustion predicted by the EDM doesn't lead to a complete consumption of reaction educts. In Fig. 6 to Fig. 9, the concentrations of the main simulation species are shown for the two combustion models at several axial cuts. Within the hot regions, the part of C_4H_6 and O_2 in the EDM calculations is higher. Even in the flame zone, a small amount of educts remains. There, the largest differences to the WD calculations occurred, which result from the temperature deviation.

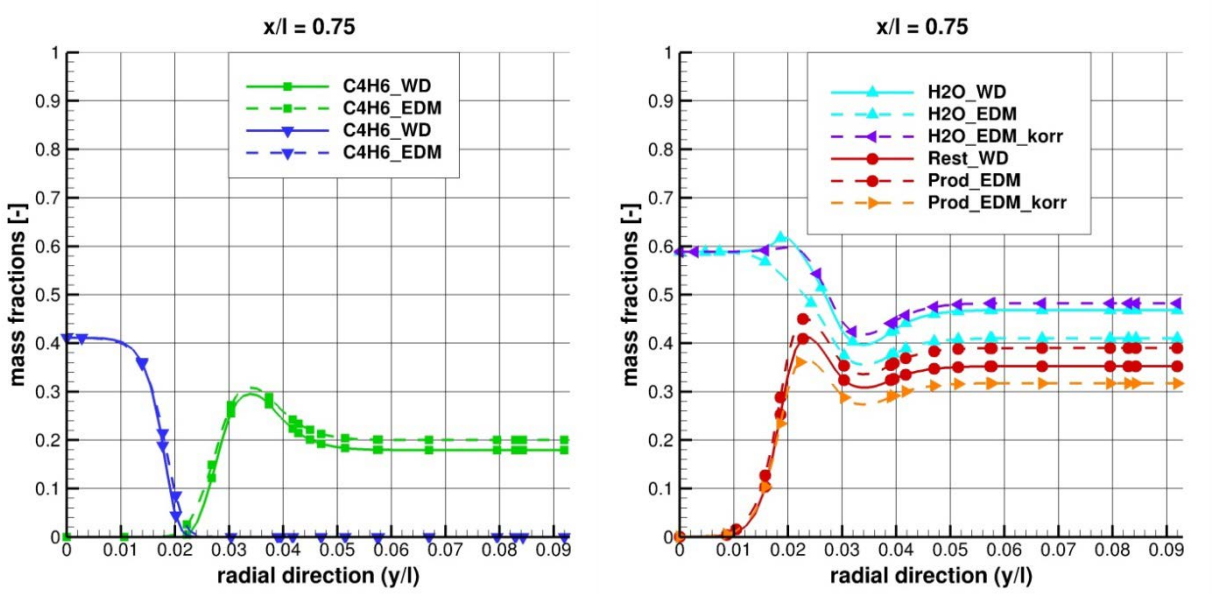

Figure 8: Comparison of the main reaction species distribution between the EDM and the WD mechanism in a axial cut at x/l=0.75 (post-combustion chamber); left: C_4H_6 and O_2; right: H_2O and products

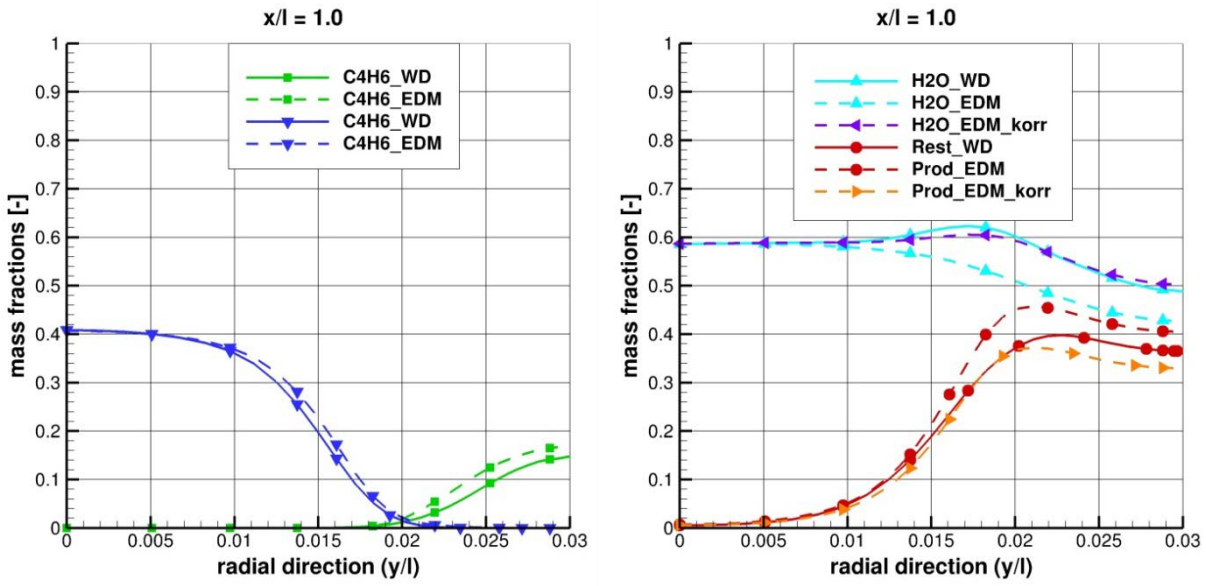

Figure 9: Comparison of the main reaction species distribution between the EDM and the WD mechanism in a axial cut at x/l=1.0 (nozzle exit); left: C_4H_6 and O_2; right: H_2O and products

Since the model specie *Prod* partly consists of H_2O, the by the EDM predicted amount of H_2O is significant lower and the amount of products is higher. With a mass fraction correction, the part of products is lower compared to the WD calculations and in hot regions, the amount of H_2O is a bit higher. The last fact is founded by the neglect of dissociation within the EDM, but the effect is low. The smaller amount of products caused by the incomplete combustion, as discussed above.

DOI: 10.13009/EUCASS2017-157

5. Conclusions

First results of the EDM simulations show good agreements with the simulations, carried out with the multistage combustion model of WD. Only a small difference of maximum 100 K in the flame zone is shown. This caused on an incomplete propellant consumption of the EDM. To reduce this difference, the semi-empirical constants for the reaction rates should be modified and validated with several multistep combustion models. Nevertheless, the calculation quality of the presented EDM is quiet well. Therefore, it provides a high potential to reduce computing time and it looks like an important step for the simulation of unsteady combustion processes within complex hybrid rocket combustion chambers.

6. Outlook

As next step, the EDM will be compared with other Arrhenius based reaction models. In addition, different O/F ratio calculations will be carried out to validate the model for general combustion cases. Furthermore, the simulation will be coupled with a pressure and temperature dependent regression rate model. Therefore, a new boundary condition for the fuel pyrolysis will be designed. Due to this, it should be possible to calculate local surface temperatures and fuel mass flow rates.

References

[1]: Božić, O., D. Porrmann, D. Lancelle and A. Hartwig. 2012. Program AHRES and its contribution to assess features and current limitations of Hybrid Rocket Propulsion. *International Astronautical Congress.* IAC-12-C4.2.8.

[2]: Westbrook, C. K. and F. L. Dryer. 1981. Simplified Reaction Mechanisms for the Oxidation of Hydrocarbon Fuels in Flames. *Combustion Science and Technology*. Vol. 27, pp. 31-43.

[3]: May, S. and O. Božić. 2015. CFD Simulation of Chemical Non-Equilibrium Reacting Flow within the AHRES Hybrid Rocket Engine. *6th European Conference for Aeronautics and Space Sciences (EUCASS).* Krakow, Poland.

[4]: May, S. and O. Božić. 2016. Numerical Simulation of the Flow and Combustion Inside the Reaction Chamber of the AHRES Hybrid Rocket Engine. *In: Dillmann, A. et al.: Notes on Numerical Fluid Mechanics and Multidisciplinary Design 132 - New Results in Numerical and Experimental Fluid Mechanics X*. Springer. ISBN 978-3-319-27278-8.

[5]: Menter, F. R., M. Kuntz and R. Langtry. 2003. Ten Years of Industrial Experience with the SST Turbulence Model. *Turbulence, Heat and Mass Transfer 4 – Proceedings of the Fourth International Symposium on Turbulence, Heat and Mass Transfer*. Antalya, Turkey.

[6]: May, S., D. Lancelle and D. Porrmann. 2013. Mathematical Modeling of a high test peroxide catalyst chamber fpr hybrid rocket engines. *13th ONERA_DLR Aerospace Symposium.* Palaiseau, France.

[7]: Božić, O., D. Porrmann, D. Lancelle and S. May. 2016. Enhanced development of a catalyst chamber for the decomposition of up to 1.0 kg/s hydrogen peroxide. *CEAS Space Journal*. Vol. 8, No. 2, pp. 77-88. DOI 10.1007/s12567-015-0109-x.

[8]: Chiaverini, M. 2007. Review of Solid-Fuel Regression Rate Behavior in Classical and Nonclassical Hybrid Rocket Motors. *In: Fundamentals of Hybrid Rocket Combustion and Propulsion - Progress in Astronautics and Aeronautics.* Vol. 328, AIAA Inc.

[9]: Chiaverini, M., G. C. Harting, Y. Lu, K. K. Kuo, A. Peretz, H. S. Jones, B. S. Wygle, and J. P. Arves. 1999. Pyrolysis Behavior of Hybrid-Rocket Solid Fuels Under Rapid Heating Conditions. *Journal of Propulsion and Power*. Vol. 15, No. 6, pp. 888-895.

[10]: Porrmann, D., O. Božić, D. Lancelle, and S. May. 2013. Regression Rate Models versus experimental Results for Hybrid Rocket Engines based on H2O2 and HTPB/Al. *64th International Astronautical Congress.* IAC 13.C4.2.10.

[11]: Gordon, S., and B. J. McBride. 1971. Computer Program for Calculation of Complex Chemical Equilibrium Compositions, Rocket Performance, Incident and Reflected Shocks and Chapman-Jouguet Detonations. NASA SP-273.

[12]: Spalding, D.B. 1971. Mixing and chemical reaction in steady confined turbulent flames. *13th symposium (international) on combustion, The combustion institute*, pp. 649–657.

[13]: Magnussen, B. F. 2005. The Eddy Dissipation Concept a Bridge Between Science and Technology. *ECCOMAS Thematic Conference on Computational Combustion*.